The [(DT-TTF)$_2$M(mnt)$_2$] Family of Radical Ion Salts: From a Spin Ladder to Delocalised Conduction Electrons That Interact with Localised Magnetic Moments

Elisabet Ribera,[a] Concepció Rovira,*[a] Jaume Veciana,[a] Judit Tarrés,[a] Enric Canadell,[a] Roger Rousseau,[a] Elies Molins,[a] Montserrat Mas,[a] Jean-Philippe Schoeffel,[b] Jean-Paul Pouget,[b] Jorge Morgado,[c] Rui T. Henriques,[c] and Manuel Almeida[d]

Abstract: Electrocrystallisation of the π-electron donor dithiopheno-tetrathiafulvalene (DT-TTF) with maleonitrile dithiolate (mnt) – metal (M) complexes gives rise to the new family of radical ion salts [(DT-TTF)$_2$M(mnt)$_2$] (M = Au, Pt, Ni), which are isostructural and crystallise in the monoclinic space group $P2_1/n$ forming regular segregated stacks of donor and acceptor molecules along the *b* axis. The DT-TTF stacks are paired and interact strongly through S···S contacts in a ladder-like motif. The three salts have quite high room-temperature electrical conductivities (9, 40 and 40 S cm^{-1} for M = Au, Pt and Ni respectively) but their conductivity – temperature dependencies differ. The Au salt has an activated conductivity at room temperature whereas the Ni and Pt salts are metal-like at room temperature and both exhibit a metal – insulator transition around 120 K. These contrasting transport properties are accounted for by the differences in the transfer integrals along the DT-TTF stacks. The magnetic susceptibility of the salt with M = Au, in which the [Au(mnt)$_2^-$] anion is diamagnetic, can be fitted to a two-legged spin-ladder model. From diffuse X-ray scattering studies it is established that below 220 K the donors dimerise along the *b* stacking direction, and the spin carrier units in the ladder are identified as those formed by dimerised donors [(DT-TTF)$_2$]$^{+\bullet}$. Observation in their EPR spectra of a single line which increases dramatically in width as the conductivity increases is evidence for the presence of two magnetic subsystems which interact in the salts (M = Ni, Pt) with paramagnetic [M(mnt)$_2$]$^-$ ions.

Keywords: conducting materials · crystal engineering · magnetic properties · spin ladder · tetrathiafulvalenes

Introduction

Since the discovery of metallic properties in molecular organic compounds, a large variety of such materials based on planar π-electron donor molecules has been synthesised,[1] some of which exhibit different ground states and new physical phenomena, depending on composition, temperature, pressure and magnetic field.[1, 2] The metallic radical cation salts with paramagnetic anions are particularly interesting, since the co-existence of delocalised conduction electrons and localised magnetic moments raises the possibility of new physical phenomena resulting from their mutual interaction.[3]

The synthesis and characterisation of one-dimensional (1D) chain-like and two-dimensional (2D) layered organic conductors are well documented, and in some crystals both electronic dimensionalities can co-exist.[4] Nevertheless, compounds with an intermediate dimensionality (that is, a finite number of assembled stacks, next to each other, forming ladders) are very uncommon and are receiving much attention, especially in the area of quantum magnets.[5–8]

Among the 1D organic metals, the structure of the α phases of the [(per)$_2$M(mnt)$_2$] family of compounds (per = perylene; mnt = maleonitrile dithiolate; M = transition metal) can be described as two regular stacks of partially oxidised perylene molecules, (per)$^{0.5+}$, next to each other, surrounded by four regular stacks of [M(mnt)$_2$]$^-$ counterions.[9] The interstack perylene – perylene interactions are extremely small com-

[a] Dr. C. Rovira, E. Ribera, Prof. J. Veciana, Dr. J. Tarrés, Prof. E. Canadell, Dr. R. Rousseau,[+] Dr. E. Molins, Dr. M. Mas
Institut de Ciència de Materials de Barcelona (CSIC)
Campus Universitari, E-08193, Bellaterra (Spain)
Fax: (+34) 935805729
E-mail: c.rovira@icmab.es

[+] Present address: National Research Council of Canada, Ottawa K1A 0R6 (Canada)

[b] J.-P. Schoeffel, Prof. J.-P. Pouget
Laboratoire de Physique des Solides (CNRS-URA02), Batiment 510
F-91405 Orsay (France)

[c] Dr. J. Morgado, Dr. R. T. Henriques
Departamento de Engenharia Química, Instituto Superior Técnico
Av. Rovisco Pais, P-1049 – 001 Lisboa (Portugal)

[d] Prof. M. Almeida
Dep. Química, Instituto Tecnológico e Nuclear
P-2686-953 SACAVÉM Codex (Portugal)

  0947-6539/99/0507-2025 $ 17.50+.50/0

pared with the strong intrastack interactions;[10] consequently, these compounds are metals with an enhanced 1D character.[3b, 11] In order to achieve a ladder-type molecular organic compound, we replaced the perylene donor by the sulfur-rich donor dithiopheno-tetrathiafulvalene (DT-TTF) **1**,[12] to com-

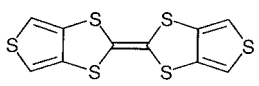

DT-TTF

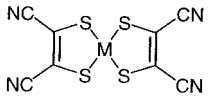

$[M(mnt)_2]$

bine with the $[M(mnt)_2]^-$ ions. This donor retains the planarity and aromatic character of perylene but incorporates six peripheral sulfur atoms that can establish intercolumn S···S contacts. The crystal structure of neutral DT-TTF shows stacks of molecules with short S···S and C–H···S interstack contacts that promote a 2D crystal packing.[13] We have used both diamagnetic and paramagnetic $[M(mnt)_2]^-$ counterions to obtain a new family of compounds in which delocalised conduction electrons and non-magnetic or localised magnetic centres can co-exist.

In this paper we report the synthesis and the structural and physical characterisation of the new family of compounds $[(DT\text{-}TTF)_2M(mnt)_2]$ (M = Au, Pt, Ni). The salt with M = Au has a diamagnetic anion whereas those with M = Ni and Pt have paramagnetic anions (square-planar Ni^{III} and Pt^{III} complexes have a spin $S = ½$). In the $[(DT\text{-}TTF)_2Au(mnt)_2]$ salt the unpaired electrons are localised on the interacting pairs of donor stacks, isolated one from another by stacks of anions. The magnetic properties of this compound show that the localised electrons behave as a two-legged spin-ladder system;[14] this is one of the first reported examples of molecular materials that exhibit this uncommon property.[15–17] It is isostructural with the salts with the paramagnetic $[Pt(mnt)_2]^-$ and $[Ni(mnt)_2]^-$ ions, but they exhibit a metal-like behaviour at room temperature due to the delocalisation of the electrons on the DT-TTF stacks. Interestingly, these electrons interact strongly with the paramagnetic anions.

Abstract in Catalan: *L'electrocristal·lització del donador d'electrons π ditiofè-tetratiafulvalè (DT-TTF) amb complexes de metalls de transició (M) del maleonitrilditiolat (mnt) dóna lloc a la nova família de sals d'ió radical $[(DT\text{-}TTF)_2M(mnt)_2]$ (M = Au, Pt, Ni). Aquestes sals són isoestructurals i cristal·litzen en el grup espacial monoclínic $P2_1/n$ formant apilaments regulars i segregats de molècules de donador i d'acceptor al llarg de l'eix b. Els apilaments de DT-TTF s'aparellen formant una escala mitjançant interaccions fortes S···S intermoleculars. Les tres sals tenen conductivitats força elevades a temperatura ambient (9, 40 i 40 $S\,cm^{-1}$ per M = Au, Pt i Ni respectivament) però presenten diferents dependències amb la temperatura. La sal d'Au té una conductivitat activada a temperatura ambient, mentre que les sals de Pt i Ni són metàl·liques a temperatura ambient i ambdues presenten una transició metall–aïllant al voltant de 120 K. Les diferències en les propietats de transport són conseqüència dels diferents valors de les integrals de transferència al llarg dels apilaments de DT-TTF. La susceptibilitat magnètica de la sal amb M = Au, en la qual l'anió $[Au(mnt)_2]^-$ és diamagnètic, es pot ajustar a un model d'escala de spin de dues potes. Mitjançant experiments de difracció difusa de raigs X s'ha establert que per sota de 220 K els donadors dimeritzen al llarg de l'eix d'apilament b, la qual cosa permet l'assignació de les unitats portadores de spin en l'escala a les formades per dímers de donadors $[(DT\text{-}TTF)_2]^{+\bullet}$. Les sals amb M = Ni i Pt en les que els anions $[M(mnt)_2]^-$ son paramagnètics, tenen dos subsistemes magnètics que interaccionen entre ells, fet evidenciat per l'observació d'una sola línia en els espectres de RPE, l'amplada de la qual augmenta dràsticament al augmentar la conductivitat.*

Results and Discussion

Crystal structure: The Au, Ni and Pt salts are isostructural and crystallise in the monoclinic space group $P2_1/n$. The asymmetric unit of the unit cell contains one DT-TTF molecule and half of the $[M(mnt)_2]$ species. Their molecular structures are depicted in Figure 1 and the crystallographic data are given in

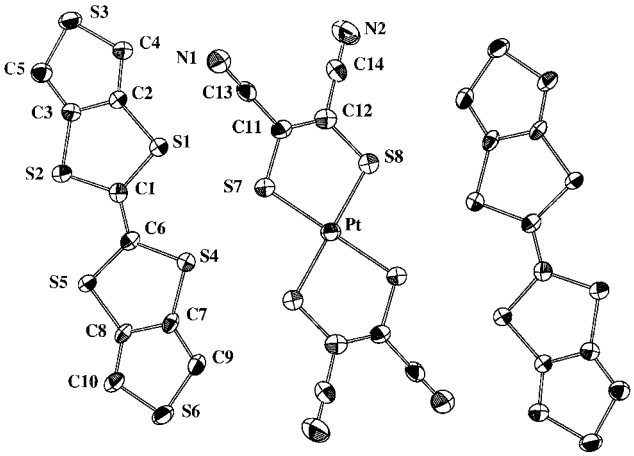

Figure 1. Molecular structure of the $[(DT\text{-}TTF)_2Pt(mnt)_2]$ salt.

Table 1. The DT-TTF and $[M(mnt)_2]$ units are essentially planar and form regular segregated donor and acceptor stacks along the *b* axis in a herringbone pattern (Figure 2a). The DT-TTF and $[M(mnt)_2]$ units are tilted with respect to the stacking axis *b*. The dihedral angles of the DT-TTF planes with the *b* axis are 24.9°, 22.4° and 22.12° and those of the $[M(mnt)_2]$ planes are 24.3°, 21.5° and 17.5° for the Au, Ni and Pt salts, respectively.

The interplanar distances are given in Table 2. Donor molecules overlap in all three compounds by slipping in the direction parallel to the shortest axis of the molecule (Figure 3a), as in the structure of the neutral donor.[13] The overlap mode of the $[M(mnt)_2]$ units is slightly different for the three salts (Figures 3b–3d): in the Pt salt it is closer to a metal-over-metal arrangement and in the Ni salt it is closer to a metal-over-sulfur situation, although the latter structure is not so clearcut as that observed for the perylene analogue.[9c] These different overlap modes are expected to be relevant for different magnetic interactions between $[M(mnt)_2]$ units.

0947-6539/99/0507-2026 $ 17.50+.50/0 *Chem. Eur. J.* **1999**, *5*, No. 7

Table 1. Crystallographic data of $[(DT\text{-}TTF)_2M(mnt)_2]$ salts

M	Au	Pt	Ni
formula	$C_{28}H_8S_{16}N_4Au$	$C_{28}H_8S_{16}N_4Pt$	$C_{28}H_8S_{16}N_4Ni$
molecular mass	1110.3	1108.4	972.0
T [K]	293	293	293
dimensions [mm]	$0.37 \times 0.23 \times 0.065$	$0.50 \times 0.05 \times 0.03$	$0.60 \times 0.04 \times 0.01$
space group	$P2_1/n$	$P2_1/n$	$P2_1/n$
a [Å]	16.334(1)	16.304(5)	16.277(2)
b [Å]	3.912(1)	3.803(5)	3.830(1)
c [Å]	27.348(2)	28.015(5)	27.811(4)
α [°]	90.0	90.0	90.0
β [°]	101.787(6)	102.29(3)	102.63(1)
γ [°]	90.0	90.0	90.0
volume [Å^3]	1710.7(2)	1697(2)	1691.8(5)
Z	2	2	2
ρ_{calcd} [g cm^{-3}]	2.16	2.17	1.91
scan mode	ω-2θ	ω-2θ	ω-2θ
intervals h, k, l	± 23, 0–5, -39–0	± 22, 0–5, 0–39	± 18, -4 to 0, -31 to 0
$2\theta_{max}$ [°]	61.9	60.7	47.3
measured reflections	7898	5248	3076
independent reflections	5444	5151	2565
R	0.0275	0.0504	0.0511
wR	0.2780	0.1106	0.1032

The DT-TTF stacks are arranged in pairs related by a twofold screw axis parallel to the b axis, and alternate with single stacks of $[M(mnt)_2]$ units along the a–c direction (Figure 2). This crystal packing is very similar to that of the α-

Abstract in French: *L'électrocristallisation du donneur à électrons π DT-TTF (dithiopheno-tetrathiafulvalene) avec les complexes métalliques (M) du maléonitriledithiolate (mnt) donne naissance à une nouvelle famille de sels à ions radicaux [(DT-TTF)$_2$ M(mnt)$_2$] (M = Au, Pt, Ni). Ces sels isostructuraux cristallisent dans le groupe d'espace monoclinique P2$_1$/n, en formant, le long de la direction b, des colonnes régulières ségrégées de molécules donneuses et acceptrices d'électrons. Les colonnes de DT-TTF sont appariées deux par deux, en échelles, par de fortes interactions intermoléculaires S···S. Ces sels présentent une assez forte conductivité électrique à température ambiante (9, 40 et 40 S cm^{-1} pour M = Au, Pt et Ni respectivement) avec toutefois d'assez différentes dépendances en température. Le sel d'Au a une conductivité activée thermiquement tandis que les sels de Ni et Pt, de type métallique à température ambiante, présentent une transition métal–isolant vers 120 K. Ces propriétés de transport contrastées peuvent être corrélées à des différences d'intégrales de transfert le long des colonnes DT-TTF. La susceptibilité magnétique du sel d'Au, dans lequel l'anion [Au(mnt)$_2$]$^-$ est diamagnétique, peut être ajustée par un modèle d'échelle de spins à deux montants. Les expériences de diffusion diffuse des rayons X établissent que, en dessous de 220 K, les molécules donneuses se dîmérisent dans la direction d'empilement b, ce qui montre que les unités de spin des échelles sont situées dans les dimères [(DT-TTF)$_2$]$^{+\bullet}$. Les sels avec M = Ni and Pt, dans lesquels l'anion [M(mnt)$_2$]$^-$ est paramagnétique, présentent deux sous systèmes magnétiques en forte interaction, comme le prouve la détection d'une seule raie de résonance paramagnétique électronique; la largeur de cette raie croissant fortement avec la conductivité.*

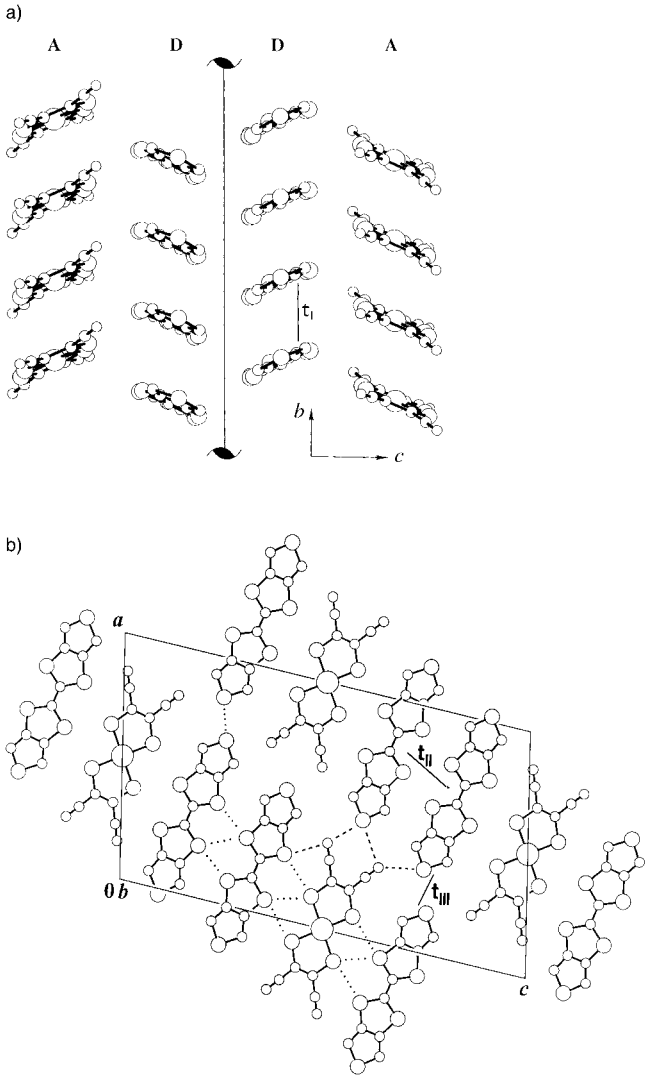

Figure 2. Crystal structure of $[(DT\text{-}TTF)_2Pt(mnt)_2]$: a) projection along a; b) view perpendicular to the (a, c) plane of the structure showing short S···S (••••) and S···N (- - - -) contacts.

Table 2. Interplanar distances [Å] in the DT-TTF and $[M(mnt)_2]$ stacks

M	dt stacks	$[M(mnt)_2]$ stacks
Au	3.555(3)	3.581(4)
Pt	3.527(4)	3.636(4)
Ni	3.534(3)	3.568(3)

$[(per)_2M(mnt)_2]$ salts.[9a–c] However, at variance with the perylene salts, due to the six sulfur atoms on the periphery of the DT-TTF molecules, the pairs of donor stacks related by the screw axis are strongly connected by three close interstack S(2)–S(5) contacts (Figure 2b and Table 3). As a result of these short contacts, the pairs of donor stacks form a structural two-legged ladder (Figure 2). This arrangement is very similar to the 2D organisation found in the crystal structure of the neutral donor;[13] the crystal packing of these $[(DT\text{-}TTF)_2M(mnt)_2]$ salts can be described formally as derived from the DT-TTF crystal structure by introducing one stack of anions between each two stacks of donors, thus cutting the 2D arrangement and giving rise to the two-legged

ladder structure. The pairs of donor stacks are connected along the *a* axis by one short S(6)–S(6iii) contact. The $[M(mnt)_2]$ molecules also play an important role in the crystal packing by establishing significant S···S and S···N interactions with the sulfur atoms of the DT-TTF molecules (Figure 2b, Table 3).

Optical properties and determination of the charge on the ions: The stoichiometry of the $[(DT\text{-}TTF)_2M(mnt)_2]$ salts was found to be (DT-TTF)/$M(mnt)_2$ = 2:1 by elemental and X-ray crystal structure analyses. If the metal complex acceptors are assumed to have a monoanionic character, this stoichiometry implies an average partial oxidation state of the donor DT-TTF of +0.5 if the charge on the anions remains unaltered during the formation of the salts. The mixed-valence character of the three salts was confirmed by the presence of the characteristic broad A band in the IR and Vis/NIR spectra, corresponding to the mixed-valence states of low-dimensional conducting organic solids,[18] centred at 3320, 3500 and 3700 cm^{-1} for the

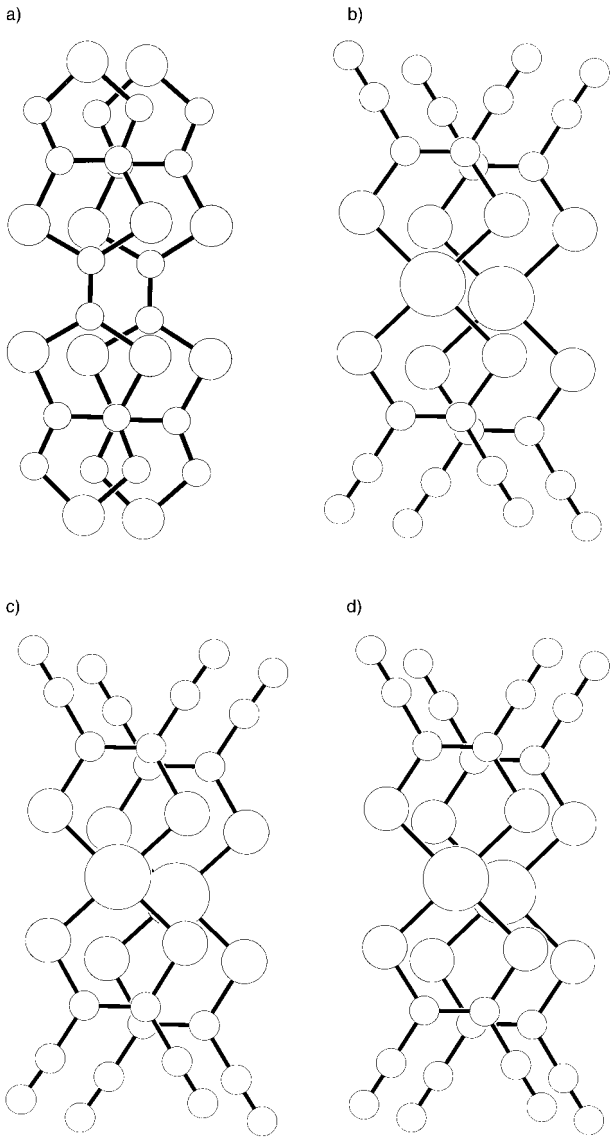

Figure 3. Overlap mode of a) DT-TTF; and of $[M(mnt)_2]$ units with b) M = Au, c) M = Ni and d) M = Pt.

Abstract in Portuguese: *A electrocristalização do doador electrónico π, DT-TTF (ditiofeno-tetratiofulvaleno) com complexos de metais de transição (M) e maleonitriloditiolato (mnt), permite obter uma nova família de sais de ião radical $[(DT\text{-}TTF)_2M(mnt)_2]$ (M = Au, Ni e Pt). Estes sais são isoestruturais e cristalizam no grupo $P2_1/n$ do sistema monoclínico, formando empilhamentos regulares e segregados de moléculas de doadores e aceitadores ao longo do eixo b. Os empilhamentos de DT-TTF estão emparelhados e interactuam fortemente através de contactos S···S formado uma estrutura em escada. Os três sais apresentam uma condutibilidae eléctrica à temperatura ambiente relativamente elevada (9, 40 e 40 $S\,cm^{-1}$ respectivamente para M = Au, Pt e Ni) mas com diferentes dependências térmicas. O composto de ouro apresenta uma condutibilidade eléctrica que à temperatura ambiente é termicamente activada à enquanto que os sais de Pt e Ni apresentam um comportamento de tipo metálico com transição metal–isolador a cerca de 120 K. Estas diferentes propriedades de transporte são explicadas pelas diferenças nos integrais de transferência electrónica ao longo dos empilhamentos de DT-TTF. A susceptibilidade magnética do sal de Au, em que o anião $[Au(mnt)_2]^-$ é diamagnético, pode ser bem ajustada a um modelo de spins em escada simples. Experiências de dispersão difusa de raios-x neste composto mostram que abaixo de 220 K os doadores se dimerizam ao longo do eixo b dos empilhamentos, permitindo a atribuição das unidades com spins na escada aos doadores dimerizados $[(DT\text{-}TTF)_2]^{+\bullet}$. Os sais de Pt e Ni, em que os aniões $[M(mnt)_2]^-$ são paramagnéticos, apresentam dois subsistemas magnéticos em interacção, como é evidenciado pelo sinal de RPE com uma só risca, cuja largura aumenta drasticamente à medida que a condutibilidade eléctrica aumenta.*

Table 3. S···S and S···N short distances in the $[(DT\text{-}TTF)_2M(mnt)_2]$ salts.

Type of distance[a]	S···S^m (DT-TTF–DT-TTF)	S···S^m (DT-TTF–$[M(mnt)_2]$)	S···N^m (DT-TTF–$[M(mnt)_2]$)	S···S^m ($[M(mnt)_2]$–$[M(mnt)_2]$)
Au	3.599^{i} 3.912^{iii} 3.784^{i} 3.775^{iii} 3.611^{i} 3.804^{iii} 3.470^{ii}	3.724^{iii} 3.600^{iv} 3.822^{iii} 3.646 3.944^{iv} 3.760	3.378^{v} 3.428^{vi} 3.608^{vi} 3.683 3.465^{iii} 3.224^{vii}	3.912^{iii} 3.988^{iii}
Ni	3.579 3.830 3.786 3.821 3.579 3.858 3.424	3.731 3.666 3.933 3.700 4.007 3.932	3.351 3.477 3.608 3.593 3.423 3.271	3.830 3.998
Pt	3.608 3.803 3.816 3.827 3.597 3.882 3.438	3.713 3.659 3.821 3.658 3.961 3.830	3.306 3.391 3.557 3.622 3.480 3.280	3.803 4.221

[a] *m* is the symmetry operation of the neighbouring molecule for which the contact is given. Their operations correspond to: i = 1.5 − *x*, −0.5 + *y*, ·0.5 − *z*; ii = 0.5 − *x*, −0.5 + *y*, −0.5 − *z*; iii = *x*, 1 + *y*, *z*; iv = 1 − *x*, 1 − *y*, −*z*; v = 0.5 + *x*, 0.5 − *y*, −0.5 + *z*; vi = 2 − *x*, −*y*, −*z*; vii = 2 − *x*, 1 − *y*, −*z*. Those contacts where the symmetry operation, *m*, is not indicated are between atoms in the reference asymmetric unit. The *m* operations are indicated in the Au compound only; those for Ni and Pt are the same in identical dispositions.

0947-6539/99/0507-2028 $ 17.50+.50/0 *Chem. Eur. J.* **1999**, *5*, No. 7

Ni, Pt and Au salts respectively. Among the several $[M(mnt)_2]$ salts with tetrathiafulvalene derivatives as a donor[19] these are the first mixed-valence salts to be obtained. The exact valence values of the molecular components of charge transfer compounds based on the stoichiometry are controversial. For instance, the formal charges in salts such as Na-TCNQ or $[(BEDT\text{-}TTF)_2]NO_3$ (TCNQ = 7,7,8,8-tetracyanoquinodimethane; BEDT-TTF = bisethylenedithio-tetrathiafulvalene) may not correspond to the actual charge distribution in the solid.[20] Such a situation also applies in some cases when the anion has acceptor character, because some charge transfer from the donor molecule to the anion can occur during the electrocrystallisation process.[19f] Since the $[M(mnt)_2]^-$ (M = Ni, Pt) ions are good acceptors,[21] we must confirm that the charge on the anion remains unaltered during the formation of the salts, that is, that the mixed-valence character observed in the $[(DT\text{-}TTF)_2M(mnt)_2]$ salts is due to the organic part only. Some reliable methods based on IR and Raman spectroscopy as well as on geometric factors have been developed in order to determine the charge on molecules in low-dimensional conducting solids based on the more common building blocks, such as the acceptor TCNQ and donors tetrathiafulvalene (TTF) and BEDT-TTF.[20, 22, 23] Nevertheless, for compounds based on $[M(mnt)_2]$ anions, there is very little information available. Best et al. studied the relationship between the stretching modes of CN groups (ν(CN)) and the charge (-1 to -3) on the $[M(mnt)_2]^{n-}$ complexes.[24] In $[M(mnt)_2]^{n-}$ salts, the CN groups give rise to intense vibrational bands which are in general only weakly coupled to other vibrations of the molecule, and are well isolated from the vibrational modes of the donor molecule. Therefore, their frequencies can be used for the evaluation of the valence of the anion complex. It has been found (Table 4) that the ν(CN) increases by about 15 ± 1 cm^{-1} upon oxidation from the dianion to the monoanion. Comparison of the ν(CN) stretching mode values obtained for $[(DT\text{-}TTF)_2M(mnt)_2]$ salts (Table 4) with those of the starting tetrabutylammoniun salts and other $[M(mnt)_2]$ salts[24, 19f] led us to conclude that the three anions in DT-TTF derivatives have a formal charge of nearly -1, although it is difficult to estimate quantitatively the valence of $[M(mnt)_2]^{n-}$.

It is also well known that the molecular geometry varies with the electron population of the MOs in the complexes.[20] Thus, a comparison of the M–S bond lengths in neutral and charged $M[(mnt)_2]$, $[M(mnt)_2]^-$ and $[M(mnt)_2]^{2-}$ species reveals that this parameter is also very sensitive to the oxidation state of the metal, although the relationship between charge transfer and geometry is only approximate.[19f, 25] We have compared the M–S bond lengths in the $[(DT\text{-}TTF)_2M(mnt)_2]$ salts with those of other well-characterised $[M(mnt)_2]$ salts (Table 4). The great similarity between the bond lengths in the (DT-TTF)-based salts and those in the M^{III} compounds points towards a formal charge of -1 on the $[M(mnt)_2]$ complexes, in agreement with the results obtained from the values of the CN stretching modes. This means that the mixed-valence character observed spectroscopically for these compounds seems to be due to only the organic part of the salts, the DT-TTF donors.

Table 4. CN stretching frequency (ν), M–S bond lengths (d) and anion charge (n) of $[M(mnt)_2]^{n-}$ based salts.

Anion	Cation	ν(CN) [cm^{-1}]	d M–S [Å]	n	Ref.
$[Au(mnt)_2]$	solution	2213,2226		-1	24
		2195		-2	24
	Bu_4N	2208, 2222		-1	24
	Et_4N		2.307, 2.305, 2.312, 2.300,2.308, 2.309	-1	52
	perylene		2.308, 2.322	-1	53
	BEDT-TTF[a]	2222	2.308, 2.302	-1	19f
	nmpz[b]		2.327, 2.310, 2.316		54
	DT-TTF	**2204, 2216**	**2.317, 2.320**	**-1**	this work
$[Ni(mnt)_2]$	solution	2211, 2226(sh)		-1	24
		2195, 2213(sh)		-2	24
	Bu_4N	2206, 2220(sh)		-1	this work
		2197, 2216(sh)		-2	24
	Et_4N	2194(sh),2210	2.148, 2.151,2.149	-1	24, 55
		2195, 2205(sh)	2.177, 2.171	-2	24, 56
	perylene		2.146, 2.135	-1	53
	nmpz[b]		2.142, 2.141, 2.139, 2.134, 2.137	-1	57
			2.158, 2.175	-2	58
	DT-TTF	**2205**	**2.144, 2.155**	**-1**	this work
$[Pt(mnt)_2]$	solution	2204(sh), 2215		-1	24
		2189(sh), 2200		-2	24
	Bu_4N	2207	2.262, 2.256, 2.265,	-1	this work, 59
		2188(sh), 2197	2.290, 2.282	-2	24, 60
	Et_4N		2.261, 2.274, 2.270, 2.259	-1	61
	perylene	2207	2.262, 2.260	-1	53
	BEDT-TTF[a]	2194, 2181(sh)		-2	19f
	DT-TTF	**2205.0**	**2.269, 2.275**	**-1**	this work

[a] Bisethylenethio-tetrathiafulvalene. [b] *N*-Methylphenazinium.

Electrical transport properties: The ladder-type crystal packing of the DT-TTF molecules in the $[(DT\text{-}TTF)_2M(mnt)_2]$ mixed-valence salts was expected a priori to provide almost 1D metallic properties; room-temperature electrical conductivities in the range 7–40 S cm^{-1} were found (Table 5). Nevertheless, although the three salts are isostructural, their room-temperature electrical conductivities (Table 5) are significantly different and, most importantly, their temperature dependencies are distinct (Figure 4).

Table 5. Conductivity and thermopower data for $[(DT\text{-}TTF)_2M(mnt)_2]$ salts.

M	$\sigma_{r.t.}$[S cm^{-1}]	$T_{trans.}$ [K]	S [μV K^{-1}]
Au	9	220	38
Ni	40	120	50
Pt	40	127	55

The Au salt has electrical conductivity at room temperature of 9 S cm^{-1} and over the whole temperature range studied (100–300 K) the electrical conductivity decreases as the temperature is lowered. However, the rate of decrease is not independent of temperature: a broad maximum at circa 220 K occurs in the graph of $-d(\log\rho)/d(1/T)$ versus T (Figure 4 bottom).

Thermopower S (Figure 5) is positive for all three salts in the temperature range studied (75–300 K), indicating hole

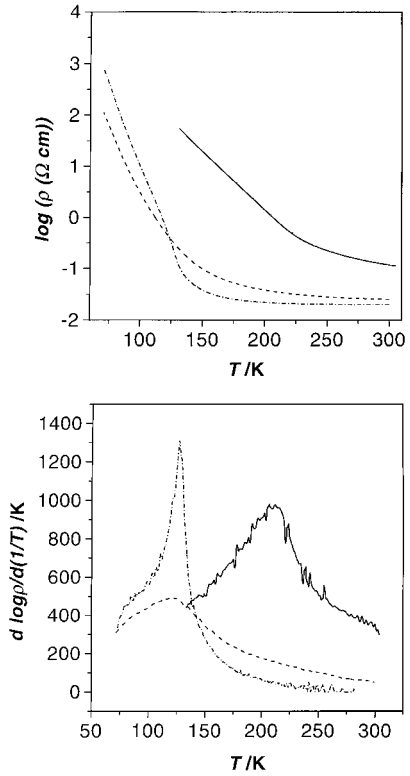

Figure 4. Variation with temperature T of $\log\rho$, measured along the b axis (top), and of $d\log(\rho)/d(1/T)$ (bottom), for $[(DT\text{-}TTF)_2M(mnt)_2]$ with M = Au (——), Ni (- - - -) and Pt (•–•–).

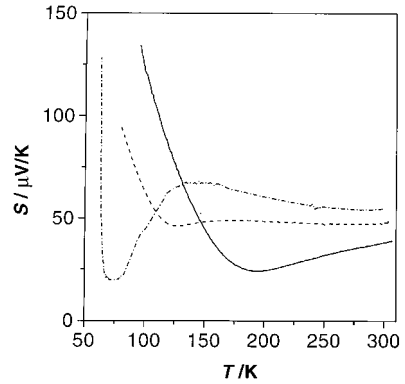

Figure 5. Absolute thermoelectric power (thermopower) of $[(DT\text{-}TTF)_2M(mnt)_2]$ with M = Au (——), Ni (- - - -), and Pt (•–•–) measured along the b axis as a function of temperature.

transport, as expected in a partially oxidised donor band. The regime with S almost proportional to the absolute temperature, observed above 200 K for the Au salt, indicates that, in this temperature range, the Fermi level lies in a continuum of states. In the same range, X-ray diffuse scattering data (see below) give evidence of dimerisation of the donor double stacks into small domains which may be separated by non-dimerised regions, where the electrons may be more delocalised, and may therefore give rise to metal-like behaviour of the thermopower. Conductivity data suggest a conduction hopping mechanism between the regions of less-delocalised states. Below 200 K, the temperature of the maximum conductivity derivative $d(\log\rho)/d(1/T)$, the thermopower increases gradually as the system is cooled, as expected in a semiconducting regime when there is a gap in the charge degrees of freedom. This change of regime is ascribed to an enhanced localisation of charge carriers which might result from the disappearance of the non-dimerised domains. This effect is discussed below in relation to the diffuse X-ray scattering data.

Near room temperature the Pt and Ni salts present a higher, temperature-independent, electrical conductivity (40 $S\,cm^{-1}$ at 300 K) than the Au salt, indicating a metal-like behaviour. Upon cooling a dramatic decrease in the conductivity is observed around 127 K for M = Pt and to a smaller extent around 120 K for M = Ni (Figure 4 top). At these temperatures $-d(\log\rho)/d(1/T)$ exhibits a maximum (Figure 4 bottom), which is particularly sharp for the Pt compound, denoting the opening of a gap. In the Pt compound diffuse X-ray scattering experiments (see below) show that the metal-to-insulator (M–I) transition observed at 127 K is associated with a structural transition.

The atypical temperature dependence of thermopower in the Pt and Ni compounds above 100 K cannot be understood on the basis of a single-band picture; it could be caused by a complex electronic structure and its modification through the M–I transition. In agreement with the electronic band structure calculations discussed below, the strong interaction between the paired donor stacks forming the ladder is expected to lead to a splitting of the donor HOMO bands that in the similar perylene compounds are degenerate.[10] Therefore, the high-temperature electrical transport properties of the $[(DT\text{-}TTF)_2Pt(mnt)_2]$ and $[(DT\text{-}TTF)_2Ni(mnt)_2]$ salts can be understood as being typical of a multiband metallic system. These two salts are the first reported metallic compounds based on a TTF-derived donor with aromatic substituents.

Electronic structure: Judging from the short S···S and S···N distances in the crystals, there are three DT-TTF···DT-TTF, one $[M(mnt)_2]\cdots[M(mnt)_2]$ and six different DT-TTF···$[M(mnt)_2]$ intermolecular interactions (two within the slabs along the $(-a + c)$ direction and four between such slabs) in the crystal structure of the $[(DT\text{-}TTF)_2M(mnt)_2]$ (M = Ni, Pt, Au) salts. Calculations for the three-dimensional (3D) lattices of these salts show that, as far as the one-electron band structures are concerned, the interactions between the HOMO of the DT-TTF donors and the LUMO of the $[M(mnt)_2]$ acceptors are very small. These interactions should certainly play a role in their magnetic properties but not in the nature of the band structure and the Fermi surface of these salts. Therefore we will consider the two subsystems separately.

The possible participation of the acceptor stacks in the conductivity is an important factor that must be considered before the differences in conductivity between the three salts, or the M–I transitions in the Ni and Pt salts, are understood. Although the on-site electron–electron repulsion (U) value associated with the $[M(mnt)_2]^-$ LUMO is not known, we calculated a bandwidth of 0.45 eV for the LUMO band of the $[Pt(mnt)_2]$ stacks in $[(DT\text{-}TTF)_2Pt(mnt)_2]$, which is very similar to that calculated with the same computational technique for the $[Pt(mnt)_2]$ LUMO band of the $[(per)_2Pt(mnt)_2]$

0947-6539/99/0507-2030 $ 17.50+.50/0 *Chem. Eur. J.* **1999**, *5*, No. 7

salt (0.39 eV)[10] and considerably smaller than that calculated for the structurally very similar $[Pt(mnt)_2]$ stacks in $[Li_{0.8}(H_3O)_{0.33}Pt(mnt)_2]$ (0.80 eV).[26] Since it is well known that the electrons in the $[Pt(mnt)_2]$ LUMO levels in $[(per)_2Pt(mnt)_2]$ are localised[9, 11] whereas those of the $[Li_{0.8}(H_3O)_{0.33}Pt(mnt)_2]$ salt are delocalised (that is, the salt is metallic),[27] our calculations give additional proof that the electrons in the $[Pt(mnt)_2]^-$ stacks (and for similar reasons those in the $[Ni(mnt)_2]^-$ stacks also) must be localised. Since the LUMO levels of the $[Au(mnt)_2]^-$ stacks in $[(DT\text{-}TTF)_2Au(mnt)_2]$ are all doubly filled, the differences in the conductivity behaviour of the three salts must arise from variations in their DT-TTF networks.

The topology of the calculated band structures for M = Pt, Au is essentially identical (Figure 6). There is significant dispersion along b^* and considerably less along a^* for both

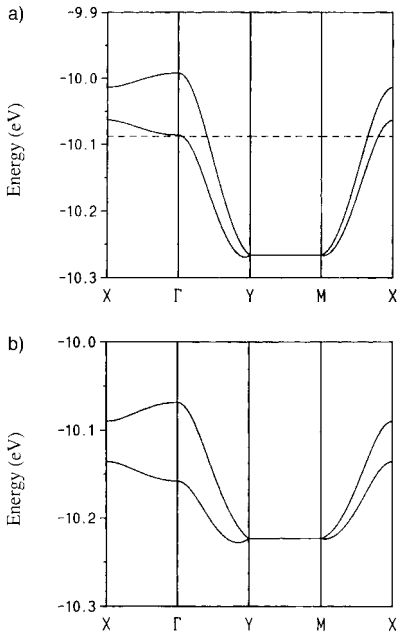

Figure 6. Dispersion relationships for the HOMO bands of the DT-TTF donor slabs of a) $[(DT\text{-}TTF)_2Pt(mnt)_2]$ and b) $[(DT\text{-}TTF)_2Au(mnt)_2]$. The band structures for the Ni and Pt salts are very similar; therefore we only report one of them here. The broken line in a) indicates the Fermi level. Γ, X, Y and M refer to the wave vectors (0, 0), (a^*/2, 0), (0, b^*/2) and (a^*/2, b^*/2), respectively. Note the different energy scales in a) and b).

systems. Both the energy separation at Γ and the dispersion in the a^* direction are essentially identical in the two salts. The only difference lies in the greater bandwidth along b^* (that is, Γ → Y) for the Pt salt. The total bandwidth (W) for the Pt salt (0.29 eV) is practically twice that for the Au salt (0.15 eV). It is well known that for a formally partially filled one-electron band situation, the metallic state is the ground state only if $W > U$.[28, 29] Since the Au salt is semiconducting whereas the Pt salt is metallic, these bandwidths suggest that the boundary between a localised electronic state ($W < U$) and a metallic state ($W > U$) is somewhere between the two salts, which is in accord with the relatively low room-temperature conductivities of these salts and the weak metallic behaviour of the Pt and Ni salts.

We now turn to the origin of the M–I transition in the Pt and Ni salts of DT-TTF. The closely related $[(per)_2M(mnt)_2]$ salts undergo an M–I transition caused by a Fermi surface instability. The calculated Fermi surface for the $[(DT\text{-}TTF)_2Pt(mnt)_2]$ salt (Figure 7 left) consists of two pairs of non-equivalently warped lines running along a direction perpendicular to b^* (that is, the stacking direction). Clearly, there is no single vector nesting the whole Fermi surface, and consequently the M–I transition is not a classical Fermi-surface-driven structural instability. This situation is somewhat puzzling because even if, as we have argued, the electronic structures of these salts are on the borderline between localised and delocalised, at least for the Pt salt the phase transition seems not to be due to a classical electronic localisation phenomenon because the resistivity versus temperature upturn is too abrupt.

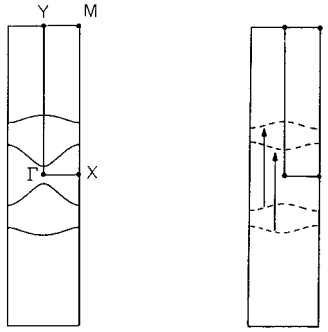

Figure 7. Left: Calculated Fermi surface for the DT-TTF donor slabs of $[(DT\text{-}TTF)_2Pt(mnt)_2]$; that for the Ni salt is almost identical. Right: Schematic illustration of the Fermi surface when the transfer integral t_{III} is reduced (a small reduction of t_{II} also has been assumed).

To understand the possible origin of the transition we must consider the different transfer integrals in the DT-TTF sublattice. As mentioned, there are three different DT-TTF ··· DT-TTF interactions (Figure 2): I) those within the DT-TTF molecular stacks along the b axis; II) those connecting the two molecular stacks related by the screw axis, and forming a pair; III) those between the extremities of the molecules in different paired stacks. Among the calculated transfer integrals ($t_{HOMO\text{–}HOMO}$) for M = Ni, Pt, Au (Table 6), t_{II} and t_{III} are practically identical for all three salts. Integral t_{III} controls the dispersion along the a^* direction and thus the warping of the two different lines of the Fermi surface. Integral t_{II} controls the separation between the two bands at Γ and consequently the separation between the two different warped lines of the Fermi surface. The large values of t_I are related to the overlap between the p orbitals of the carbon atoms of the central double bond and those of the sulfur

Table 6. Calculated transfer integrals [meV] in $[(DT\text{-}TTF)_2M(mnt)_2]$ salts.

M	t_I	t_{II}	t_{III}
Au	36	21	6
Ni	55	21	6
Pt	64	20	6

atoms of the TTF moiety (see Figure 3a for the overlap mode); t_I is considerably smaller for M = Au because of the increase of 0.11 Å in the length of the *b* axis (see below). Integral t_I controls the dispersion along the *b** direction and is the factor ultimately responsible for the difference in the conductivity of the Pt/Ni and Au salts.

Thus, inclusion of sulfur atoms in the donor introduces two major differences from the $[(per)_2M(mnt)_2]$ salts. In the latter, t_{II} and t_{III} are both negligible, so the Fermi surface is just the superposition of two practically ideal straight lines separated by ¼*b**. Consequently, the $[(per)_2M(mnt)_2]$ salts are ideally suited to exhibiting a Fermi surface instability leading to a structural modulation with wave vector $\boldsymbol{q} = ¼b^*$.[29, 30] In the Fermi surface of the DT-TTF salts the S···S interactions lead to separation of the two lines of every pair, and to the straight lines becoming warped with opposite curvature. Yet, there is still the possibility of some kind of structural modulation with wave vector $\boldsymbol{q} = ¼b^*$ which can open a gap all along the Fermi surface. As we noted, the dispersion along the *a** direction, and thus the different curvature of the lines in the Fermi surface, are due to the t_{III} transfer integral. This integral is small, however, and quite weak structural changes affecting the S···S contact between paired stacks (see Figure 2b) will decrease it. When t_{III} is decreased the two lines become flatter and more equivalent, as shown schematically in Figure 7 right. In that case, a single nesting vector ($\boldsymbol{q} = ¼b^*$, imposed by the stoichiometry) can nest the whole Fermi surface and thus lead to an M–I transition. However, without reduction of t_{III} by the initial structural change, structural modulation driven by the Fermi surface will not occur. Thus, this mechanism can be described as a structurally assisted $2k_F$ instability. Alternatively, the reduction in t_{III} could be brought about simply by thermal contraction. In order to distinguish between the two possibilities it would be necessary to determine the crystal structure for a temperature slightly above the M–I transition, so that the corresponding Fermi surface could be calculated. In any case, the Fermi surface instability is not predictable from the room-temperature Fermi surface. This situation, first discussed in order to explain the M–I transition in $[(BEDT\text{-}TTF)_2ReO_4]$, is referred to as hidden Fermi surface nesting.[31, 32]

There is still another possible (and probably more likely) mechanism for the M–I transition. As discussed above, these salts lie at the borderline between localised and delocalised electronic structures and a small reduction in the t_I transfer integral would be enough for them to fall into the localised regime. If this reduction happened, the natural chemical units bearing the unpaired electrons are $(DT\text{-}TTF)_2$ dimers (see X-ray scattering section, below). This situation must lead to some kind of dimerisation (either with short- or long-range order) along the stacking direction. However, why should this reduction of t_I occur? It can be argued that thermal contraction would most probably lead to a decrease in the interplanar DT-TTF···DT-TTF distance, and thus to an increase in t_I. There are two important parameters that affect the geometric dependence of t_I [taking as starting values those of the Pt salt (Table 6)]: the interplanar separation and the sliding of one of the DT-TTF donors along its short axis. Bearing in mind the differences between the Pt and Au salts in the interplanar distance (0.03 Å shorter for M = Pt) and the donor sliding along the short axis (0.21 Å greater for M = Au), we studied in detail how t_I depends on these two geometric parameters. Our main conclusions are: i) reduction of the interplanar distance leads to an increase in t_I (for instance, for a reduction of 0.03 Å t_I is increased by 6 meV); ii) sliding of the donors along the short molecular axis away from each other leads to a decrease in t_I (for instance, sliding by 0.09 Å leads to a reduction in t_I of 14 meV). Our results suggest that a very small sliding motion of the order of magnitude of 0.2 Å could easily change the t_I transfer integral from the value for the Pt or Ni salts towards that for the Au salt, that is, from the values appropriate for the delocalised regime to those for the localised regime. The smaller value of t_I (Table 6) for the Au salt (and thus, the semiconducting behaviour) is due to the increase in both the interplanar separation and the sliding of the donors away from each other. However, as can be understood easily from the data reported above, the role of the sliding is clearly dominant.

As thermal contraction probably has the effect of decreasing the separation between the planes of the DT-TTF donors, this decrease will raise the value of t_I. However, according to our study, this effect can be more than compensated by a small sliding of the two donors away from each other along the direction of their short axis. Consequently, an abrupt small sliding motion of the two donors could also be the driving force for an M–I transition in these salts. Since in that case some kind of dimerisation would result, this mechanism would just be a $4k_F$ instability of the donor slabs.[33] The tendency towards this $4k_F$ instability, which we believe is inherent in the $[(DT\text{-}TTF)_2]^{+\cdot}$ networks in these salts, could be enhanced by any type of instability leading to dimerisation in the $[Pt(mnt)_2]$ stacks. The diffuse X-ray scattering measurements (see below) strongly suggest that this scenario is the most likely one for the Pt salt. Such a dimerisation of the $[Pt(mnt)_2]$ stacks, coupled with a $4k_F$ instability of the donor stacks, would also be consistent with the magnetic susceptibility and EPR data (see Magnetic properties section), which differ markedly from the data for the Ni salt.

From the results of Figure 4 (top), it is clear that the change from the initial pseudo-metallic to the semiconducting regime is much more progressive for M = Ni than for M = Pt. This suggests that thermal contraction brings about a progressive electron localisation within the DT-TTF stacks. Two factors probably contribute to the difference in behaviour of the M = Pt and M = Ni salts: i) with the slightly smaller t_I, the M = Ni salt is nearer the boundary between the localised and delocalised states; ii) the $4k_F$ instability of the DT-TTF stacks is not assisted by a tendency towards dimerisation in the $[Ni(mnt)_2]^-$ stacks (as discussed in the Crystal structure section).

Magnetic properties: Since the $[Au(mnt)_2]^-$ anion is diamagnetic, the paramagnetic properties of the $[(DT\text{-}TTF)_2\ Au(mnt)_2]$ salt result from the spins on the DT-TTF paired stacks, whereas in the other two salts (M = Ni, Pt) there are contributions from the two magnetic subsystems: the DT-TTF paired stacks, with mobile electrons; and the $[M(mnt)_2]$ stacks, with localised spins.

For the salt with the diamagnetic anion $[Au(mnt)_2]^-$, the static paramagnetic susceptibility (χ_p) and effective magnetic

0947-6539/99/0507-2032 $ 17.50+.50/0 *Chem. Eur. J.* **1999**, *5*, No. 7

moment (μ_{eff}), measured by the Faraday method in the range 2–300 K and assuming a diamagnetic contribution of 4.6×10^{-4} emu mol^{-1} (estimated from tabulated Pascal constants), are plotted against T in Figure 8. The high value of the

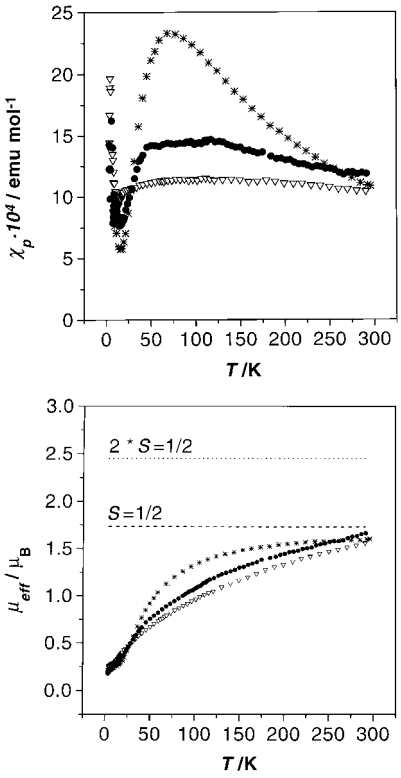

Figure 8. Temperature dependence of the paramagnetic susceptibility χ_P (top) and the effective magnetic moment μ_{eff} (bottom) of [(DT-TTF)$_2$M(mnt)$_2$] with M = Au (*), Ni (●) and Pt (▽).

effective moment (μ_{eff} = 1.60 μ_B at room temperature) clearly indicates that there is one spin per [(DT-TTF)$_2$Au(mnt)$_2$] formula unit and, moreover, that the electrons in the DT-TTF units are already localised at this temperature, in agreement with the transport properties. The average X-ray structure previously described does not reveal in which entities the electrons are localised, but when the X-ray scattering results (vide infra) are taken into account, one can consider the spin carrier units to be those formed by dimerised donors $[(DT\text{-}TTF)_2]^{+\bullet}$, with $S = ½$. After the structural interactions, such dimerised donors can interact magnetically with the neighbouring spin carrier units in a ladder model, as represented schematically in Figure 9, where $J_\parallel$ and $J_\perp$ are the exchange coupling constants along the legs and along the rungs of the ladder, respectively.

The temperature dependence of the static paramagnetic susceptibility does not show any significant anomaly around 220 K. The absence of anomalies in this temperature region where the transport properties do change indicates that, as a consequence of electronic correlations in the DT-TTF stacks, separation of the spin and charge degrees of freedom occurs in this system. The temperature dependence of the magnetic susceptibility exhibits a maximum around 70 K with activated behaviour below this temperature crossing over to a Curie–Weiss form at higher temperatures. This $\chi(T)$ plot is characteristic of a system having localised $S = ½$ spins with antiferro-

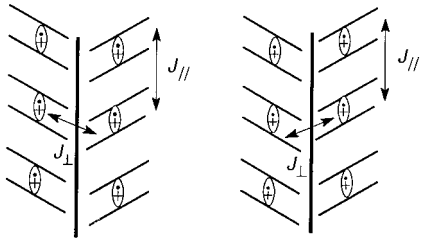

Figure 9. Schematic illustration of the two possible two-legged ladders formed by the dimerisation of the DT-TTF stacks in [(DT-TTF)$_2$Au(mnt)$_2$], where $J_\parallel$ is the exchange coupling along the legs and $J_\perp$ is the coupling along the rungs of the ladder.

magnetic interactions together with a gap in the low-temperature region. In accordance with the structural characteristics, the best fit of the data from 8 to 45 K has been achieved with the low-temperature expression [Eq. (1)] for the susceptibil-

$$\chi_{ladder} = \alpha T^{-1/2} \exp(-\Delta/k_B T) \quad (1)$$

ity of a spin-ladder model given by Troyer et al.,[34] where α is a constant corresponding to the dispersion of the excitation energy, and Δ is the finite energy gap in the spin-excitation spectrum. For such a fit, the Curie contribution χ_{Curie}, which takes into account both the finite size of the spin ladders and the magnetic defects present in the crystals (molar fraction f), was introduced [Eq. (2)].

$$\chi = f\chi_{ladder} + (1-f)\chi_{Curie} \quad (2)$$

The parameters resulting from this fit were $f = 0.98$, $\alpha = 7.22 \times 10^{-4}$ emu K$^{1/2}$ mol^{-1}, and $\Delta/k_B = 78$ K ($r^2 = 0.9972$). Fitting all the data (Figure 10) to the two-legged ladder model

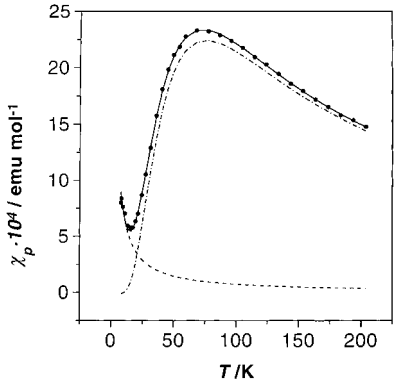

Figure 10. The paramagnetic susceptibility (●) of the [(DT-TTF)$_2$-Au(mnt)$_2$] salt as a function of temperature. The solid line is the fit by Equation (2) to a contribution of a spin-ladder model (•–•–) and a Curie tail (- - - -) (see text).

equations given by Barnes and Riera [Eq. (3)][35] gives the exchange coupling parameters $J_\parallel/k_B = -83$ K and $J_\perp/k_B = -142$ K, with $f = 0.980$ ($r^2 = 0.9989$).

$$\chi_{ladder}(T) = \frac{c_1}{T}\left[1 + \left(\frac{T}{c_2}\right)^{c_3} (e^{c_4/T} - 1)\right]^{-1}\left[1 + \left(\frac{c_5}{T}\right)^{c_6}\right]^{-1} \quad (3)$$

The ratio $J_\parallel/J_\perp$ agrees qualitatively with the ratio of the transfer integrals evaluated from the t_I and t_{II} values when the

dimeric nature of the elementary building block of the spin ladder has been taken into account (Figure 9). The spin gap has also been calculated from the resulting values of $J_{\parallel}$ and $J_{\perp}$ by the theoretical expression (4),[32] giving $\Delta/k_B = 83$ K, in good agreement with the previous value.

$$\Delta = |J_{\perp}| - |J_{\parallel}| + J_{\parallel}^2/2|J_{\perp}| \quad (4)$$

The EPR spectrum of an oriented single crystal of the $[(DT\text{-}TTF)_2Au(mnt)_2]$ salt is characterised by a single resonance line with a Lorentzian shape. Both the peak-to-peak linewidth (ΔH_{pp}) and the g factor values exhibit a sinusoidal dependence on the angle of the applied magnetic field, the extreme values of the g factor being 2.0021, 2.0052 and 2.0131, which are almost identical to those found in the salt $[(DT\text{-}TTF)_2Re_6S_5Cl_9 \cdot 2C_3H_7NO]$, where strongly coupled, singly oxidised $[(DT\text{-}TTF)_2]^{+\cdot}$ dimers exist,[36] and agree with the molecular orientations of the radical cations in the crystal. Thus, the minimum g value observed for this salt is close to the free-electron value of 2.0023, as expected for any planar sulfur π-donor radical cation with the axis perpendicular to the molecular plane oriented parallel to the applied magnetic field (H_0), where the contribution of the spin–orbit coupling is very small.[37] On the other hand, the maximum g value is found when H_0 is parallel to the a^* crystallographic axis, which corresponds approximately to the long axis of the donor molecule (see Figure 2b), as is usually observed for oxidised TTF derivatives.[38] In addition, the average g factor of a polycrystalline sample ($g = 2.0064$) is very similar to that observed for the free radical cation in solution under isotropic conditions ($g_{iso} = 2.0077$).[13a] It is also interesting that the anisotropy of the ΔH_{pp} parameter gives values for the three crystal orientations of 25, 26 and 43 G which are consistent with the α-like packing of the DT-TTF donors in the crystal lattice. Thus it is clear that the EPR signal is due only to the oxidised DT-TTF donor species, confirming the diamagnetic nature of the monoanionic $[Au(mnt)_2]$ complexes.

The thermal variation of the g factor and ΔH_{pp} parameters, and of the EPR signal intensity (I) observed when the magnetic field is parallel to the b^* axis, are displayed in Figure 11. The intensity of the EPR signal closely follows the spin-ladder behaviour observed for the static magnetic susceptibility (Figure 8). As for the static magnetic susceptibility, no change in the EPR parameters is observed around 220 K, the temperature region where the conductivity shows a transition.

The magnetic behaviour of the $[(DT\text{-}TTF)_2M(mnt)_2]$ salts containing magnetic anions (M = Ni, Pt), where two different kinds of spin carrier co-exist, is very distinct from that of the Au salt (Figure 8). In both Ni and Pt salts the effective magnetic moment μ_{eff} shows a continuous decrease when the temperature is lowered, indicating an antiferromagnetic coupling between the spins (Figure 8 bottom). The presence of sizeable antiferromagnetic interactions is also indicated by the low values of μ_{eff} at room temperature ($1.56\mu_B$ for Pt, $1.66\mu_B$ for Ni), since this value is very similar to that of the Au salt ($1.60\mu_B$), in spite of the presence of the extra paramagnetic $[M(mnt)_2]^-$ centres. This cannot be explained only

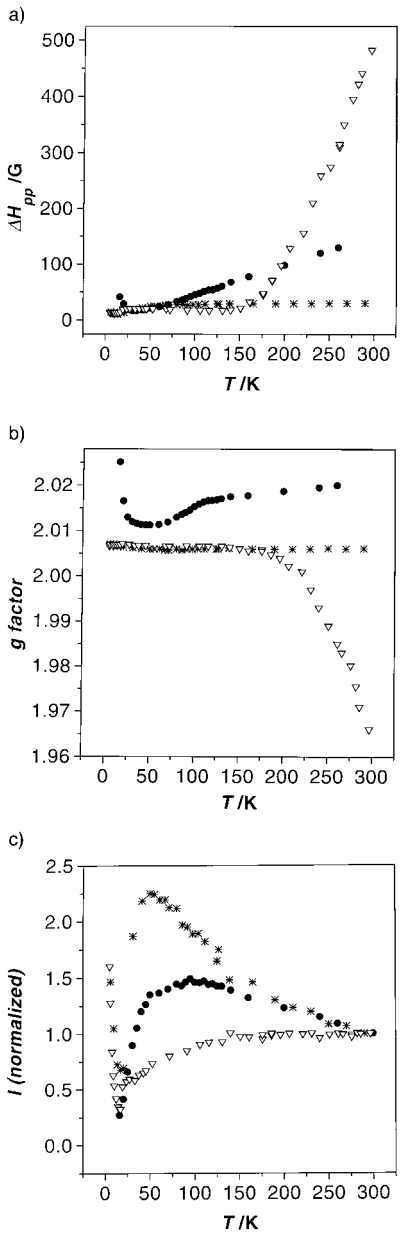

Figure 11. Temperature dependence of EPR parameters of $[(DT\text{-}TTF)_2M(mnt)_2]$ single crystals for M = Au (*) and Ni (°), and a polycrystalline sample for M = Pt (▽): a) ΔH_{pp}; b) g factor; c) intensity of the EPR signal.

by the reduction in the paramagnetic contribution from the DT-TTF stacks due to the higher electron delocalisation (Pauli-like behaviour) since, as shown by the electronic band calculations, the donor bandwidth is small. The plot of the paramagnetic susceptibility χ_p against T for Ni and Pt salts (Figure 8 top) has a very flat profile at high temperature, especially for the Pt salt. In both compounds there is a sharp anomaly in the susceptibility at lower temperatures (at circa 50 K for Ni, 20 K for Pt), followed by an exponential decrease, indicating a magnetic transition, possibly to a spin–Peierls or an antiferromagnetic state. The nature of this transition is unclear. Above the transition temperature, the susceptibility of either salt could not be fitted to any simple magnetic model, such as an antiferromagnetic dimer or chain model, nor to a two-legged spin-ladder model or known 2D models (quad-

0947-6539/99/0507-2034 $ 17.50+.50/0 *Chem. Eur. J.* **1999**, *5*, No. 7

ratic and hexagonal layers).[39] The flat susceptibility profile suggests the presence of a complex 2D or 3D network of non-regular antiferromagnetic interactions or a system with frustrated antiferromagnetic interactions. The crystal packing of the [DT-TTF$_2$M(mnt)$_2$] salts accounts for this high-dimensional magnetic character since there are short S···S contacts along the three directions linking molecules of the same or different natures (Figure 2 and Table 3). These contacts are very important for the magnetic interactions because sulfur atoms of both types of molecules have high spin densities, as revealed from their SOMO (single occupied molecular orbital). No anomaly is observed for the susceptibility of the Pt compound (like the Au salt) in the M–I transition temperature region. In the Ni compound the M–I transition corresponds to a very small change in slope of $\chi_p(T)$ in the M–I transition temperature region. The same susceptibility behaviour is indicated by the variation of the intensity of the EPR spectra with T in a single crystal of the Ni salt and in a polycrystalline sample of the Pt salt (Figure 11c).

The EPR spectra of the Pt salt over the whole temperature range studied (4–300 K), and of the Ni salt above 15 K, all consist of a single line. In contrast to the Au salt, the EPR lines of the Ni and Pt salts at room temperature are very broad, with linewidths ΔH_{pp} in polycrystalline samples of 210 and around 600 G respectively. At room temperature the average g factor of the Ni salt (2.0163) is between those of the [DT-TTF]$^{+\bullet}$ and [Ni(mnt)$_2$]$^-$ units ($g_{DT} = 2.0077$,[13] $g_{Ni(mnt)_2} = 2.0377$,[40] $g_{Pt(mnt)_2} = 2.0420$[41]) whereas, surprisingly, the g value of the Pt salt (1.96) is much lower than those of the [DT-TTF]$^{+\bullet}$ and [Pt(mnt)$_2$]$^{-\bullet}$ units. For both compounds a strong narrowing of the line is observed as the temperature decreases, as well as important changes in the g factors (Figure 11). Thus, the linewidth of the Ni salt decreases when it is cooled to 30 K, where ΔH_{pp} begins to increase suddenly, and the signal becomes less intense and almost vanishes. At very low temperatures, below 15 K, some narrow and very anisotropic signals appear that grow upon cooling. The g factor also decreases on cooling but its slope changes clearly at the metal insulator transition at 120 K, then has a broad minimum centred at 50 K. Below 25 K a dramatic increase of the g value is observed. The increases in linewidth and g value at low temperatures are consistent with an antiferromagnetic transition, which is responsible for the drop in the susceptibility below 50 K. This hypothesis is further supported by the appearance of additional lines, which can be attributed to antiferromagnetic resonance.

A strong decrease of linewidth and an increase of g factor occur when the Pt salt is cooled from room temperature, with a large change in slope around the T_{M-I} at 130 K. Qualitatively the signal intensity follows the susceptibility behaviour. In contrast to the Ni salt, no extra narrow line appears at very low temperatures.

As mentioned, the Pt and Ni salts have two magnetic subsystems. The observation that their EPR spectra both consist of a single line, with a dramatic increase in width and change in g values upon warming above the T_{M-I}, indicates that there is a strong interaction between the two subsystems, at least at high temperatures. The loose dependence of the linewidth on the conductivity suggests that the interaction between the [M(mnt)$_2$]$^{-\bullet}$ localised spins is mediated through the conduction electrons. This effect is probably related to the short S···S contacts shown in the crystal structure between molecules of the two subsystems (Table 3).

Diffuse X-ray scattering: To relate the electronic anomalies to structural modifications, diffuse X-ray scattering experiments were performed on Au and Pt salts which should also provide information on the transformation into a spin ladder of the structurally regular ladder of the partially oxidised DT-TTF molecules in the Au salt. For the latter purpose it was necessary to locate the units bearing the localised spin, since these entities are not clearly revealed by the average X-ray structure previously described.

In the Au salt, X-ray patterns taken at 15 K exhibit a weak scattering consisting of several single diffuse lines, each located midway between successive layers of main Bragg reflections perpendicular to the stacking direction, b. This diffuse scattering is more clearly revealed by a microdensitometer reading along b^* (inset, Figure 12). Its reduced wave

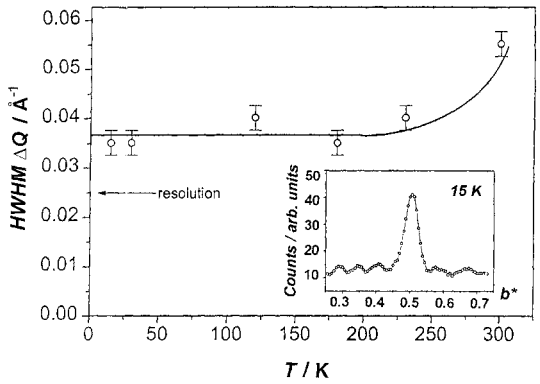

Figure 12. Thermal dependence of the HWHM of the diffuse lines of [(DT-TTF)$_2$Au(mnt)$_2$] measured along b. Inset: the microdensitometer reading along b^* of one such diffuse line, showing that its reduced wave vector is $\frac{1}{2}b^*$ (intensity in arbitrary units).

$\frac{1}{2}b^*$, indicates that dimerisation is achieved in the stacking direction. However, these lines are broader than the experimental resolution, which means that the dimerisation occurs only on a local scale. At 15 K the half-width-at-half-maximum (HWHM) of the diffuse scattering in the stacking direction is $\Delta Q = 0.035$ Å^{-1}. The inverse of this quantity, corrected by the (Gaussian) resolution of 0.025 Å^{-1}, leads to an intrastack correlation length $\xi_b = 60(40)$ Å, if one assumes an intrinsic Lorentzian (Gaussian) profile of the diffuse scattering. Weaker and broader diffuse lines can still be detected at room temperature. The diffuse lines begin to broaden substantially above about 225 K (Figure 12); at 295 K $\xi_b \simeq$ 20 Å.

The diffuse lines detected in the Au salt are of quite weak intensity. A previous study of the [(per)$_2$M(mnt)$_2$] salts[29] and that of [(DT-TTF)$_2$Pt(mnt)$_2$] (see below) show that, because of the presence of the heavy atom M, much more intense diffuse lines are observed when the dithiolate stack undergoes a structural instability. This suggests that the diffuse lines arise from a dimerisation of the DT-TTF stack. However, a definite

proof of this statement requires a structure factor analysis which is difficult to perform because of the weak intensity of the diffuse scattering.

The intensity of the diffuse lines is slightly modulated for transverse components of the scattering wave vector. This indicates that there is a phase relationship between the dimerisations on neighbouring stacks. More quantitatively the HWHM of the intensity modulation leads, at 15 K, to a correlation length of $\xi_\perp \approx 10$ Å. $\xi_\perp$ exceeds the transverse dimension (approximately 5.5 Å) of a double stack of DT-TTF donors along the rung of the ladder. This indicates that each ladder is made of coherently dimerised pairs of dimerised DT-TTF stacks. $\xi_\perp$, however, is slightly less than the centre-to-centre distance of first-neighbour ladders.

The diffuse lines observed on the X-ray patterns correspond to the intersection of the Ewald sphere with diffuse sheets in reciprocal space. The presence of the diffuse sheets means that the dimerisation is basically uncorrelated between neighbouring chain-like units; this unit begins, in our interpretation of the data, at the DT-TTF ladder. In this case, however the doubling of the b periodicity must break the 2_1 two-fold screw axis symmetry of the average structure (Figure 2) which relates the two DT-TTF stacks forming the ladder. There are two ways to break this 2_1 symmetry (Figure 9); each possibility corresponds to a different phasing between the dimerisations of the two stacks forming the ladder. On a given ladder the two kinds of phasing will occur with the same probability in different domains. Between two adjacent domains there is a break in the structural coherence of the dimerisation. From the previous determination of the intrastack correlation length, ξ_b, one can estimate that the average length of a coherently dimerised domain is $L_b = \pi\xi_b = 150$ Å (that is, $40b$) below 225 K. Two different phasings are connected by a domain wall consisting of undimerised DT-TTF molecules. If it is assumed that the domain walls contain a few unpaired DT-TTF units $S = ½$ which do not contribute to the singlet ground state, the presence of a small molar fraction f of Curie spins in the magnetic susceptibility can be explained simply.

As there is an average of half a hole per DT-TTF molecule, the dimerisation leads to the localisation of one hole per dimer. As mentioned above, this localisation can be the result of a $4k_F$ charge density wave (CDW) response of the donor stacks expected from the simultaneous presence of important electron–electron repulsions on (and between) the DT-TTF molecules and of a small intrastack electronic transfer t_I. In agreement with this interpretation, the low-temperature resistivity and thermopower show a gap in the charge degrees of freedom. The rapid decrease in the correlation length of the $4k_F$ CDW distortion above 225 K (see the inverse of this quantity, Figure 12) should lead to a significant reduction of the charge localisation effect, which is consistent with the thermal dependence of the resistivity (Figure 4) and of the thermopower (Figure 5) above about 200 K. In this model there is an $S = ½$ spin associated with each hole localised on a $[(\text{DT-TTF})_2]^{+\bullet}$ dimer. This $S = ½$ dimer interacts with all the neighbouring dimers of the DT-TTF double stack, as represented schematically in Figure 9, where $J_\parallel$ and $J_\perp$ are the coupling along the legs and the rungs of the spin ladder respectively. In principle, another interstack coupling is present. However, this coupling, which links more shifted dimers with only a single t_{III} interstack interaction, is much weaker than the previous one and can be neglected.

The $[(\text{DT-TTF})_2\text{Pt(mnt)}_2]$ salt was also investigated by diffuse X-ray scattering. As for the Au salt, diffuse lines located midway between successive layers of main reflections perpendicular to the stacking direction, b, are also detected above 130 K. Their reduced wave vector in this direction, $½b^*$, also indicates the presence of an instability towards a stack dimerisation. However, the diffuse lines of the Pt salt differ from those previously observed for the Au salt by their much stronger intensity and their temperature dependence. Their intensity and structure factor bear some resemblance to those previously detected in $[(\text{per})_2\text{Pt(mnt)}_2]$ (see Figure 5 in ref. [29]). This is a clear indication that the dimerisation occurs on the $[\text{Pt(mnt)}_2]$ stack, or in both the $[\text{Pt(mnt)}_2]$ and DT-TTF stacks. On cooling, these broad diffuse lines begin to be detected from around 250 K, and sharpen; at 100 K (Figure 13) they have already condensed into well-resolved

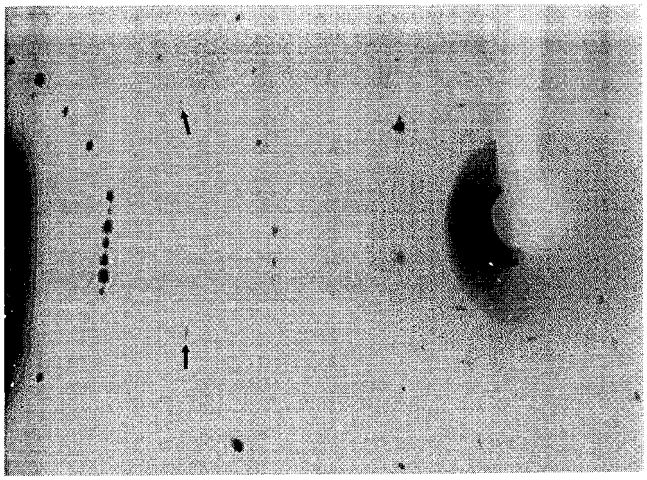

Figure 13. X-ray patterns for $[(\text{DT-TTF})_2\text{Pt(mnt)}_2]$ showing the presence at 100 K of satellite reflections from the condensation of the diffuse lines midway between layers of Bragg reflections perpendicular to the stack axis, b (horizontal direction of the pattern).

satellite reflections. Therefore, the anomaly at 127 K in the resistivity measurements (Figure 5b) must be associated with a structural transition. Sharp satellite reflections are also detected down to 50 K. At 20 K these reflections exhibit a surprising broadening in directions perpendicular to the stacking axis. At 10 K they become so broad that they have merged into modulated diffuse lines perpendicular to the b direction. This unexpected behaviour was reproduced during a second thermal cycle through the 127 K phase transition. However, after an additional cycle the sharp satellite reflections previously observed at 100 K were transformed into diffuse lines.

Let us first consider the high-temperature behaviour, say above 50 K. At 127 K, the Pt salt undergoes an M–I transition, with the opening of a gap in the charge degrees of freedom (Figure 5), accompanied by a 3D lattice dimerisation. Although the X-rays detect mainly the distortion of the $[\text{Pt(mnt)}_2]$ stacks, the gap is certainly opened on the DT-TTF

0947-6539/99/0507-2036 $ 17.50+.50/0 *Chem. Eur. J.* **1999**, *5*, No. 7

stacks because there is already one electron localised per $[Pt(mnt)_2]$ unit. The unexpected feature of this phase transition is that the spin degrees of freedom (Figure 8) do not reveal a gap opening. Thus, from the electrical and magnetic measurements, this transition cannot be due to a standard Peierls nesting mechanism of the Fermi surface (such as the one represented in Figure 7 right). This transition most probably corresponds to a charge localisation preserving the spin degree of freedom. By analogy with our previous finding for the Au salt, the localisation of one hole per DT-TTF dimer requires the dimerisation of the donor stacks. However, the X-ray pretransitional fluctuations show that the dimerisation is achieved through a 1D instability of the $[Pt(mnt)_2]$ stack. Thus the 127 K phase transition cannot be driven by a simple spin–Peierls mechanism, because the dimerisation of the dithiolate stacks does not lead to a sizeable spin gap opening. As discussed above, this result implies that the driving force of the phase transition must certainly involve the divergence of the $4k_F$ CDW response function of the donor stacks, and that the dimerisation of the dithiolate stacks must be accompanied by a dimerisation of the donor stacks in order to achieve the $4k_F$ localisation of one hole per DT-TTF dimer. In this respect, the EPR data suggest that the interaction between the $[Pt(mnt)_2]$ localised spins is mediated through the holes on the donors.

The surprising feature of the very-low-temperature structural data is the loss of transverse coherence between the intrastack dimerisations. This unexpected behaviour requires further experimental confirmation. However, it is interesting that this structural modification seems to be associated with the opening of a gap in the spin degrees of freedom (Figure 8).

Summary and Conclusions

The π-electron donor DT-TTF forms mixed-valence conducting salts with interesting magnetic and electronic properties with the transition metal complex counterions $[M(mnt)_2]^-$ (M = Au, Pt, Ni). These 2:1 salts are isostructural and crystallise in segregated stacks, with two paired and strongly interacting donor stacks forming ladders that are isolated from each other by anion stacks.

The Au salt has an activated conductivity at room temperature with an increased charge localisation below 220 K. In contrast, the Ni and Pt salts are metal-like at room temperature and both exhibit an M–I transition around 120 K. These differences in the transport properties are accounted for by the differences in the transfer integrals along the DT-TTF stacks so that the Ni and Pt salts, which have a larger bandwidth, are in the delocalised regime whereas the Au analogue, with a smaller bandwidth, is in the Mott–Hubbard insulator regime.

The paramagnetic properties of the M = Au salt, where the $[Au(mnt)_2]^-$ ion is diamagnetic, are due to the unpaired electrons of the donor stacks. The magnetic susceptibility of this salt can be fitted to a two-legged spin-ladder model. It therefore constitutes one of the first organic systems recognised as a spin-ladder material.[42]

The salts (M = Ni, Pt) with paramagnetic $[M(mnt)_2]^-$ ions have two interacting magnetic subsystems, as shown by EPR measurements in which the width of the single line is observed to increase dramatically as the conductivity increases. Both salts show antiferromagnetic interactions (2D or 3D) and at lower temperatures exhibit a transition, of a nature not yet fully understood, most probably antiferromagnetic in the Ni salt and possibly of a spin–Peierls type in the Pt salt. Further low-temperature diffuse X-ray scattering experiments are expected to clarify the nature of these transitions.

Thus the dramatic changes in the magnetic and electrical properties observed in this family of isostructural compounds may be attributed either to the change from diamagnetic to paramagnetic anions, and/or to small differences in the intermolecular overlap between DT-TTF donors.

Experimental Section

Sample preparation: $[(DT\text{-}TTF)_2M(mnt)_2]$ (M = Au, Pt Ni) crystals were obtained by electrocrystallisation from dichloromethane solutions of the donor and the tetrabutylammonium salt of $[M(mnt)_2]^-$ as electrolyte, in approximately stoichiometric amounts, with Pt electrodes and in galvanostatic conditions. The current was typically 1 μA for electrodes 1 cm long, of 1 mm diameter. DT-TTF was synthesized as previously described[13a] and purified by recrystallisation in dichloromethane/hexane. The $[Bu_4N][M(mnt)_2]$ salts were prepared as previously described,[43] and purified by recrystallisation from acetone/2-butanol. After about eight days of electrocrystallisation the dark, metallic, shiny, needle-shaped crystals, typically up to $5 \times 0.5 \times 0.1$ mm^3, were collected, and washed with dichloromethane.

$[(DT\text{-}TTF)_2Au(mnt)_2]$: $C_{28}H_8S_{16}N_4Au$: calcd C 30.29, H 0.73, N 5.04, S 46.20; found C 30.22, H 0.66, N 4.96, S 46.07.

$[(DT\text{-}TTF)_2Ni(mnt)_2]$: $C_{28}H_8S_{16}N_4Ni$: calcd C 34.59, H 0.82, N 5.76, S 52.67; found C 34.62, H 0.76, N 5.91, S 52.79.

$[(DT\text{-}TTF)_2Pt(mnt)_2]$: $C_{28}H_8S_{16}N_4Pt$: calcd C 30.34, H 0.73, N 5.05, S 46.27; found C 30.69, H 0.70, N 5.01, S 46.70.

X-ray crystal structure analysis: Single-crystal diffraction data were collected at room temperature on an Enraf–Nonius CAD4 diffractometer equipped with an Mo X-ray tube and a graphite monochromator to select the $Mo_{K\alpha}$ radiation (absorption coefficient $\mu = 5.31$ mm^{-1}). Corrections were made for Lorentz polarisation and absorption effects (DI-FABS: max/min absorption factors 1.254/0.793). The structures were refined by full-matrix least-squares methods (SHELXL-93). The minimised function was $\omega(F_o^2 - F_C^2)^2$ with $\omega = 1/\sigma^2F^2 + (AP)^2 + BP$, $P = [\mathrm{Max}(0,F_o) + 2F_c]/3$ and σ (the standard deviation) was estimated from counting statistics.
Crystallographic data (excluding structure factors) for the structures reported in this paper have been deposited with the Cambridge Crystallographic Data Centre as supplementary publication nos. CCDC-100375, CCDC-103112 and CCDC-103113. Copies of the data can be obtained free of charge on application to CCDC, 12 Union Road, Cambridge CB2 1EZ, UK (fax: (+44) 1223-336-033; e-mail: deposit@ccdc.cam.ac.uk).

Transport measurements: Electrical conductivity and thermoelectric power measurements were performed in the range 20–320 K along the *b* axis (long axis) of the needle-shaped crystals, using the same measurement cell attached to the cold stage of a closed-cycle helium refrigerator. In a first step thermopower was measured using a slow a.c. ($\approx 10^{-2}$ Hz) technique,[44] by attaching to the extremities of the single crystal, with platinum paint (Demetron 308A), two $\phi = 25$ mm 99.99% pure Au wires (Goodfellow Metals) anchored to two quartz thermal reservoirs, in previously described apparatus,[45] controlled by a computer.[46] The oscillating thermal gradient, kept below 1 K, was measured with a differential thermocouple (Au–0.05 atoms% Fe versus chromel). The sample temperature was measured by a previously calibrated thermocouple of the same type. The absolute thermopower of the sample was obtained after correction for the absolute thermopower of the Au leads, using Huebner's data.[47]
In a second step, electrical resistivity measurements of the same sample were performed by a four-probe technique. Without removal of the crystal from the sample holder, two extra Au wires were placed on the sample in

order to achieve a four-in-line contact configuration. The sample was checked to ensure that the unnested/nested voltage ratio as defined by Schaeffer et al.[48] was below 5%. Then a current of 1 μA was passed through the sample at low frequency (77 Hz) and the voltage drop was measured with a lock-in amplifier.

EPR spectroscopy: Spectra in the range 4–300 K were obtained with an X-Band Bruker ESP 300E spectrometer equipped with a rectangular cavity operating in T102 mode, a Bruker variable-temperature unit and an Oxford EPR-900 cryostat, a field frequency lock ER 033M system and an NMR gaussmeter ER 035M. The modulation amplitude was kept well below the linewidth and the microwave power was well below saturation.

Magnetic susceptibility: Measurements in the range 2–300 K were performed using a longitudinal Faraday system (Oxford Instruments) with a 7 T superconducting magnet, under a magnetic field of 2 T and forward and reverse field gradients of 5 T m^{-1}. A polycrystalline sample (4–5 mg) was placed inside a previously calibrated thin-walled Teflon bucket. The force was measured with a microbalance (Sartorius S3D-V). Under these conditions the magnetization was found to be proportional to the applied magnetic field.

Electronic spectroscopy: Transmission measurements of finely ground KBr pellet samples (about 1 wt.%) were carried out with a Nicolet 5ZDX interferometer with Fourier transform (400–4400 cm^{-1}) and a Varian Cary 5 spectrometer (3330–20000 cm^{-1}).

Band structure calculations: In the tight-binding band structure calculations an extended Hückel Hamiltonian[49] and a modified Wolfsberg–Helmoltz formula[50] were used to calculate the non-diagonal H_{ij} matrix elements. A single-ζ atomic orbital basis set was used for C, S, H and Pt 6s and 6p. For Pt 5d, double-ζ type orbitals were used. The exponents and parameters used in the calculations were taken from previous work.[51]

Diffuse X-ray scattering: Experiments were performed, as in previous studies[29] on the [(per)$_2$M(mnt)$_2$] organic conductors, with the so-called fixed film-fixed crystal method using a monochromatized $Cu_{K\alpha}$ (λ = 1.542 Å) beam obtained after (002) reflection of the principal beam on a double-beam graphite monochromator. The principal beam was produced by a conventional X-ray generator operating either in normal conditions (40 kV, 30 mA) or at low voltage (15 kV, 40 mA) in order to eliminate the λ/2 contamination of the monochromatised beam. The data were recorded either on photographic films or on imaging plates. Two needles of the Au salt and one needle of the Pt salt, about 5 mm long in the stacking direction (*b*) and a few tenths of a millimetre in the other directions, were studied. Each needle was fixed in good thermal contact with the cold finger of a He closed-circuit cryocooler, providing regulated temperatures from 10 K to room temperature.

Acknowledgment

This work was supported in Spain by grants from the DGES (PB96-0862-CO2-01 and PB96-0859), from the Generalitat de Catalunya (1977 SGR24 and SGR96-00106) and by the TMR Program of the EC (ERBFMRX CT980181), in Portugal by PRAXIS XXI, under contract no. 2/2.1/QUI/203/94, and by a JNCIT–CSIC bilateral agreement. We thank Dr. José Vidal-Gancedo for performing the EPR experiments.

[1] a) F. Wudl, *Acc. Chem. Res.* **1984**, *17*, 227; b) *Highly Conducting Quasi-One-Dimensional Organic Crystals, Semiconductors and Semimetals*, *Vol. 27* (Ed.: E. Conwell), Academic Press, London, **1988**; c) *The Physics and Chemistry of Organic Superconductors* (Eds.: G. Saito, S. Kagoshima), Springer, Berlin, **1990**; d) J. M. Williams, J. R. Ferraro, R. J. Thorn, K. D. Carlson, U. Geiser, H. H. Wang, A. M. Kini, M.-H. Whangbo, in *Organic Superconductors, Including Fullerenes: Synthesis, Structure, Properties, and Theory*, Prentice-Hall, Englewood Cliffs (NJ), **1992**; e) *Organic Conductors; Fundamentals and Applications* (Ed: J.-P. Farges), Marcel Dekker, New York, **1994**.

[2] P. Day, M. Kurmoo, *J. Mater. Chem.* **1997**, *7*, 1291.

[3] a) L. Alcácer, *Mol. Cryst. Liq. Cryst.* **1985**, *120*, 221; b) C. Bourbonnais, R. T. Henriques, P. Wzietek, D. Kongeter, J. Voiron, D. Jérôme, *Phys. Rev. B* **1991**, *44*, 641; c) V. Gama, R. T. Henriques, G. Bonfait, M. Almeida, S. Ravy, J. P. Pouget, L. Alcácer, *Mol. Cryst. Liq. Cryst*. **1993**, *234*, 171; d) M. Matos, G. Bonfait, R. T. Henriques, M. Almeida, *Phys. Rev. B* **1996**, *54*, 15307; e) M. Y. Ogawa, B. M. Hoffman, S. Lee, M. Yudkovsky, N. M. Halpern, *Phys. Rev. Lett*. **1986**, *57*, 1177; f) G. Quirion, M. Poirier, K. K. Liou, M. Y. Ogawa, B. M. Hoffman, *Phys. Rev. B* **1986**, *37*, 4272; g) P. Day, M. Kurmoo, T. Mallah, I. R. Marsden, R. H. Friend, F. L. Pratt, W. Hayes, D. Chasseau, J. Gaultier, G. Bravic, L. Ducassse, *J. Am. Chem. Soc.* **1992**, *114*, 10722; h) H. Kobayashi, H. Tomita, T. Naito, A. Kobayashi, F. Sakai, T. Watanabe, P. Cassoux, *J. Am. Chem. Soc.* **1996**, *118*, 368; i) E. Coronado, L. Falvello, J. R. Galán-Mascarós, C. Giménez-Saiz, C. J. Gómez-García, V. Lauhkin, A. Pérez-Benítez, C. Rovira, J. Veciana. *Adv. Mater*. **1997**, *9*, 984; j) M. Kurmoo, A. W. Graham, P. Day, S. J. Coles, M. B. Hursthouse, J. L. Caulfield, J. Singleton, F. L. Pratt, W. Hayes, L. Ducasse, P. Guionneau, *J. Am. Chem. Soc*. **1995**, *117*, 12209; k) P. Cassoux, *Science* **1996**, *272*, 1277.

[4] R. Rousseau, M.-L. Doublet, E. Canadell, R. P. Shibaeva, S. S. Khasanov, L. P. Rozemberg, N. D. Kushch, E. B. Yagubskii, *J. Phys. Fr*. **1996**, *6*, 1527.

[5] Z. Hiroi, M. Takano, *Nature (London)* **1995**, *337*, 41.

[6] E. Dagotto, T. M. Rice, *Science* **1996**, *271*, 618.

[7] a) E. Dagotto, J. Riera, D. J. Scalapino, *Phys. Rev. B* **1992**, *45*, 5744; b) S. Gopalan, T. M. Rice, M. Sigrist, *Phys. Rev. B* **1994**, *49*, 8901; c) T. Barnes, J. Riera, *Phys. Rev. B* **1994**, *49*, 6817; d) S. R. White, R. M. Noack, D. J. Scalapino, *Phys. Rev. Lett.* **1994**, *73*, 882 and 886; e) C. A. Hayward, D. Poilblanc, R. M. Noack, D. J. Scalapino, W. Hanke, *Phys.Rev. Lett.* **1995**, *75*, 926.

[8] a) R. S. Eccleston, T. Barnes, J. Brody, J. W. Johnson, *Phys. Rev. Lett.* **1994**, *73*, 2626; b) T. M. Rice, S. Gopalan, M. Sigrist, *Europhys. Lett.* **1993**, *23*, 445; c) M. Azuma, Z. Hiroi, M. Takano, K. Ishida, Y. Kitaoka, *Phys. Rev. Lett.* **1994**, *73*, 3463.

[9] a) L. Alcácer, H. Novais, F. Pedroso, S. Flandrois, C. Coulon, D. Chasseau, J. Gaultier, *Solid State Commun*. **1980**, *35*, 945; b) A. Domingos, R. T. Henriques, V. Gama, M. Almeida, A. L. Vieira, L. Alcácer, *Synth. Met*. **1988**, *27*, B411; c) V. Gama, M. Almeida, R. T. Henriques, I. C. Santos, A. Domingos, S. Ravy, J. P. Pouget, *J. Phys. Chem.* **1991**, *95*, 4263; d) V. Gama, I. C. Santos, G. Bonfait, R. T. Henriques, M. T. Duarte, J. C. Waerenborgh, L. Pereira, J. M. P. Cabral, M. Almeida, *Inorg. Chem*. **1992**, *31*, 2598.

[10] L. F. Veiros, M. J. Calhorda, E. Canadell, *Inorg. Chem*. **1994**, *33*, 4290.

[11] a) M. Almeida, V. Gama, R. T. Henriques, L. Alcácer, in *Inorganic and Organometallic Polymers with Special Properties* (Ed.: R. M. Laine), Kluwer Academic Publishers, Dordrecht, **1992**, pp. 163–177; b) M. Almeida, R. T. Henriques, in *Organic Conductive Molecules and Polymers*, *Vol. 1* (Ed.: H. S. Nalwa), John Wiley, Chichester, **1997**, chapter 2, pp. 87–149.

[12] Correct name: $\Delta^{2,2'}$-bithieno[3,4-*d*]-1,3-dithiol.

[13] a) C. Rovira, J. Veciana, N. Santaló, J. Tarrés, J. Cirujeda, E. Molins, J. Llorca, E. Espinosa, *J. Org. Chem*. **1994**, *59*, 3307; b) J. J. Novoa, M. C. Rovira, C. Rovira, J. Veciana, J. Tarrés, *Adv. Mater.* **1995**, *7*, 233.

[14] C. Rovira, J. Veciana, E. Ribera, J. Tarrés, E. Canadell, R. Rousseau, M. Mas, E. Molins, M. Almeida, R. T. Henriques, J. Morgado, J.-P. Schoeffel, J.-P. Pouget, *Angew. Chem.* **1997**, *109*, 2417–2421; *Angew. Chem. Int. Ed. Engl.* **1997**, *36*, 2324–2326.

[15] H. Imai, T. Inabe, T. Otsuka, T. Okuno, K. Agawa, *Phys. Rev. B* **1996**, *54*, 6838.

[16] T. Komatsu, N. Kojima, G. Saito, *Solid State Commun.* **1997**, *103*, 519.

[17] M. Fourmigué, B. Domercq, I. V. Jourdain, P. Molinié, F. Guyon, J. Amaudrut, *Chem. Eur. J.* **1998**, *4*, 1714.

[18] J. B. Torrance, B. W. Scott, F. B. Kaufman, P. E. Seiden, *Phys. Rev. B* **1979**, *19*, 730.

[19] a) M. G. Milles, J. D. Wilson, *Inorg. Chem.* **1975**, *14*, 2357; b) R. C. Wheland, J. L. Gillson, *J. Am. Chem. Soc.* **1976**, *98*, 3916; c) F. Wudl, C. H. Ho, A. Nagel, *J. Chem. Soc. Chem. Commun.* **1973**, 923; d) F. Wudl, *J. Am. Chem. Soc.* **1975**, *97*, 1962; e) A. Underhill, J. S. Tonge, P. I. Clemenson, H.-H. Wang, J. M. Williams, *Mol. Cryst. Liq. Cryst.* **1985**, *125*, 439; f) J. Tarrés, M. Mas, E. Molins, J. Veciana, C. Rovira, J. Morgado, R. T. Henriques, M. Almeida, *J. Mater. Chem.* **1995**, *5*, 1653–1658.

[20] T. C. Ummland, S. Allie, T. Kuhlmann, P. Coppens, *J. Phys. Chem.* **1988**, *92*, 6456.

  0947-6539/99/0507-2038 $ 17.50+.50/0 *Chem. Eur. J.* **1999**, *5*, No. 7

[21] Cyclic voltammetry of the starting tetrabutylammonium salts gives $E_{1/2}([Pt(mnt)_2]^{-} \leftrightarrow [Pt(mnt)_2]^{2-} = 0.32$ V and $E_{1/2}([Ni(mnt)_2^{-}] \leftrightarrow [Ni(mnt)_2]^{2-}) = 0.35$ V vs. Ag/AgCl in CH_2Cl_2.
[22] J. S. Chappel, A. N. Bloch, W. A. Bryden, M. Maxfield, T. O. Poehler, D. O. Cowan, *J. Am. Chem. Soc.* **1981**, *103*, 2442.
[23] a) H. Kuzmany, M. Elbert, *Solid State Commun.* **1980**, *35*, 597; b) H. H. Wang, J. R. Ferraro, J. M. Williams, U. Geiser, J. A. Schueter, *J. Chem. Soc. Chem. Commun.* **1994**, 1893.
[24] S. P.Best, S. A. Ciniawsky, R. J. H. Clark, R. C. S. McQueen, *J. Chem. Soc. Dalton Trans.* **1993**, 2267.
[25] a) A. Kobayashi, Y. Sasaki, *Bull. Chem. Soc. Jpn*. **1977**, *50*, 2650; b) W. Reith, K. Polborn, E. Amberger, *Angew. Chem.* **1988**, *100*, 722; *Angew. Chem. Int. Ed. Engl*. **1988**, *27*, 699; c) I. G. Dance, P. J. Solstad, J. C. Calabrese, *Inorg. Chem.* **1973**, *12*, 2161; d) F. Knoch, G. Schmauch, H. Kisch, *Z. Kristallogr*. **1995**, *210*, 76; e) P. I. Clemenson, A. E. Underhill, M. B. Hursthouse, R. L. Short, *J. Chem. Soc. Dalton Trans.* **1989**, 61; f) J. S. Miller, J. C. Calabrese, A. J. Epstein, *Inorg. Chem*. **1989**, *28*, 4230; g) W. Clegg, S. L. Birkby, A. J. Banister, J. M. Rawson, S. T. Wait, P. Rizkallah, M. M. Harding, A. Blake, *Acta Crystallogr. Sect. C* **1994**, *50*, 28; h) W. Guntner, G. Gliemann, U. Klement, M. Zabel, *Inorg. Chim. Acta* **1989**, *165*, 51; i) A. Domingos, R. T. Henriques, V. Gama, M. Almeida, A. L. Vieira, L. Alcacer, *Synth. Met*. **1988**, *27*, B411.
[26] E. Canadell, *New J. Chem*. **1997**, *21*, 11479.
[27] A. Kobayashi, T. Mori, Y. Sasaki, H. Kobayashi, M. M. Ahmad, A. E. Underhill, *Bull. Chem. Soc. Jpn*. **1984**, *57*, 3262.
[28] *Metal–Insulator Transitions* (Ed.: N. F. Mott), Taylor and Francis, London, **1974**.
[29] R. T. Henriques, L. Alcacer, J. P. Pouget, D. Jerome, *J. Phys. C: Solid State Phys.* **1984**, 17, 5197.
[30] V. Gama, R. T. Henriques, M. Almeida, J. P. Pouget, *Synth. Met*. **1993**, *55–57*, 1677–1682.
[31] M.-H. Whangbo, J. Ren, W. Liang, E. Canadell, J. P. Pouget, S. Ravy, J. M. Williams, M. A. Beno, *Inorg. Chem*. **1992** *31*, 4169.
[32] There is another possible hidden Fermi surface mechanism. If t_{II} can be increased in such a way that the lower band becomes full and the upper band becomes half-filled, then a distortion with wave vector $\frac{1}{2}b^*$ or $\frac{1}{2}a^* + \frac{1}{2}b^*$, depending on the strength of t_{III}, would also be possible. This distortion would completely destroy the Fermi surface and thus would lead to an M–I transition. However, this possibility implies a stronger structural rearrangement than that discussed in the text and, in principle, seems less likely.
[33] J. P. Pouget, in *Highly Conducting Quasi-One-Dimensional Organic Crystals, Semiconductors and Semimetals*, *Vol. 27* (Ed.: E. Conwell), Academic Press, London, **1988**, pp. 87–214.
[34] M. Troyer, H. Tsunetsugu, D. Würtz, *Phys. Rev. B* **1994**, *50*, 13515.
[35] T. Barnes, J. Riera, *Phys. Rev. B* **1994**, *50*, 6817.
[36] J.-C. Gabriel, I. Johannsen, P. Batail, *Acta Crystallogr. Sect. C* **1993**, *49*, 1052.
[37] A. Terahara, H. Ohya-Nishigushi, N. Hirota, H. Awaji, T. Kawase, S. Yoneda, T. Sugimoto, Z. Yoshida, *Bull. Chem. Soc. Jpn.* **1984**, *57*, 1760.
[38] J. M. Williams, J. R. Ferraro, R. J. Thorn, K. D. Carlson, U. Geiser, H. H. Wang, A. M. Kini, M.-H. Whangbo, *Organic Superconductors, Including Fullerenes*, Prentice Hall, Englewood Cliffs (NJ), **1992**, p. 400.
[39] a) G. A. Baker Jr., H. E. Gilbert, J. Eve, G. S. Rushbrooke, *Phys. Lett. A* **1967**, *25*, 207; b) M. E. Lines, *J. Phys. Chem. Solids* **1970**, *31*, 101; c) P. Guionneau, J. Gaultier, D. Chasseau, G. Bravic, Y. Barrans, L. Ducasse, D. Kanazawa, P. Day, M. Kurmoo, *J. Phys.* **1996**, *6*, 1581.
[40] A. Davison, N. Edelstein, R. H. Holm, A. H. Maki, *J. Am Chem. Soc.*, **1963**, *85*, 2029.
[41] R. Kirmse, W. Dietzsh, B. V. Solovev, *J. Inorg. Nucl. Chem*. **1977**, *39*, 1157.
[42] μ^+SR experiments have recently confirmed that this compound is the first molecular material reported with a two-legged spin-ladder configuration: D. Arcon, A. Lappas, S. Margadonna, K. Prassides, E. Ribera, J. Veciana, C. Rovira, R. T. Henriques, M. Almeida, unpublished results.
[43] a) A. Davison, N. Edelstein, R. H. Holm, A. H. Maki, *Inorg. Chem.* **1963**, *2*, 1227; b) A. Davison, R. H. Holm, *Inorg. Synth*. **1967**, *10*, 8.
[44] P. M. Chaikin, J. F. Kwak, *Rev. Sci. Instrum.* **1975**, *46*, 218.
[45] M. Almeida, S. Oostra, L. Alcácer, *Phys. Rev. B* **1984**, *30*, 2839.
[46] E. B. Lopes. INETI–Sacavem, internal report, **1991**.
[47] R. P. Huebner, *Phys. Rev. A* **1964**, *135*, 1281.
[48] P. E. Schaffer, F. Wudl, G. A. Thomas, J. P. Ferraris, D. O. Cowan, *Solid State Commun*. **1974**, *14*, 347.
[49] M.-H. Whangbo, R. Hoffmann, *J. Am. Chem. Soc.* **1978**, *100*, 6093.
[50] J. Ammeter, H.-B. Bürgi, J. Thibeault, R. Hoffmann, *J. Am. Chem. Soc*. **1978**, *100*, 3686–3692.
[51] B. Pommarède, B. Garreau, I. Malfant, L. Valade, P. Cassoux, J.-P. Legros, A. Audouard, L. Brossard, J.-P. Ulmet, M.-L. Doublet, E. Canadell, *Inorg. Chem*. **1994**, *33*, 3401.
[52] J. C. Fitzmaurice, A. M. Z. Slawin, D. J. Williams, J. D. Woollins, *Polyhedron* **1990**, 1561.
[53] I. C. Santos, M. Almeida et al., personal communication.
[54] F. Kuppusamy, N. Venkatalakshmi, P. T. Manoharan, *J. Crystallogr. Spectrosc. Res.* **1985**, *15*, 629.
[55] A. Kobayashi, Y. Sasaki, *Bull. Chem. Soc. Jpn.* **1977**, *50*, 2650.
[56] C. Mahadevan, M. Seshasayee, B. V. Murthy, P. Kuppusamy, P. T. Manoharan, *Acta Crystallogr. Sect. C* **1984**, *40*, 2032.
[57] F. Kuppusamy, N. Venkatalakshmi, P. T. Manoharan, J. Crystallogr. Spectrosc. Res. **1985**, *15*, 389.
[58] H. Endres, H. J. Keller, W. Moroni, D. Nothe, *Acta Crystallogr. Sect. B* **1979**, *35*, 353.
[59] R. Kirmse, S. Saluschke, personal communication, **1996**
[60] W. Guentner, G. Gliemann, U. Klement, M. Zabel, *Inorg. Chim. Acta* **1989**, *165*, 51.
[61] P. I. Clemenson, A. E. Underhill, M. B. Hursthouse, R. L. Short, *J. Chem. Soc. Dalton Trans.* **1989**, 61.

Received: November 18, 1998 [F1451]